Journal of Organometallic Chemistry, 401 (1991) 283–294
Elsevier Sequoia S.A., Lausanne
JOM 21300

Synthesis and characterization of organotin hexacyanoferrates

Alex Bonardi, Clara Carini, Corrado Pelizzi, Giancarlo Pelizzi, Giovanni Predieri, Pieralberto Tarasconi

Istituto di Chimica Generale ed Inorganica, Università di Parma, Viale delle Scienze, 43100 Parma (Italy)

Maria Antonietta Zoroddu

Istituto per l'Applicazione delle Tecniche Chimiche Avanzate ai Problemi Agrobiologici, Via Vienna 2, 07100 Sassari (Italy)

and Kieran C. Molloy

School of Chemistry, University of Bath, Claverton Down, Bath BA2 7AY (UK)

(Received June 25th, 1990)

Abstract

The synthesis and structural characterization by IR, ESR, ^{119}Sn and ^{57}Fe Mössbauer spectroscopy, X-ray powder diffraction, and TG and DSC methods of a new series of organotin hexacyanoferrates are reported.

Introduction

As part of a general program directed at the production of heterobinuclear metal complexes, we recently reported the synthesis and the X-ray crystal structures of a series of tin-silver compounds containing both arsine and phosphine ligands [1,2] and of a new cyano-bridged organotin-iron compound [3]. As an extension of this organotin chemistry, we now report the synthesis of a family of compounds of general formula $(SnR_x)_m[Fe(CN)_6]_n$ ($x = 2$, $m = 1, 2, 3$ and $n = 1, 2$; $x = 3$, $m = 3, 4$ and $n = 1$), which are produced by the reaction of the appropriate organotin chloride with potassium hexacyanoferrate (II, III).

Cyanometallate compounds of the type $M_x[M'(CN)_6]_y$ represent an interesting class of chemical species, displaying molecular sieving properties which can be predicted on the basis of their specific structure [4–6]. Very recently, an unusual compound containing ferrocene intercalated into the zeolite-like host $[(SnMe_3)_3Fe(CN)_6]_n$ and a three-dimensional host–guest system $[(SnMe_3)_4Fe(CN)_6 \cdot 2H_2O \cdot C_4H_8O_2]_\infty$ have been described [7,8].

0022-328X/91/$03.50

The present paper describes the synthesis and structural characterization by IR, ESR, and ^{119}Sn and ^{57}Fe Mössbauer spectroscopy, X-ray powder diffraction, and TG and DSC methods of a series of six new organotin hexacyanoferrates.

Experimental

All reactants and solvents were reagent grade. Solvents were dried by standard techniques before use. $SnPh_3Cl$, $SnPh_2Cl_2$, $SnPr_3Cl$, $SnBu_2Cl_2$, $K_3Fe(CN)_6$ and $K_4Fe(CN)_6$ were used as supplied commercially.

Microanalyses (C, H and N) were made on Perkin Elmer 240 automatic equipment. Iron and tin were determined by atomic absorption spectroscopy using a Perkin Elmer 303-HGA 70 instrument. Infrared spectra were recorded in the range 4000–200 cm^{-1} using a Perkin Elmer 283B spectrophotometer. Details of Mössbauer spectrometer and related procedures have been published elsewhere [9].

The thermogravimetric analyses were made with a Perkin Elmer Delta Series TGA7 thermobalance, from 30 to 400 °C, at a rate of 20 °C/min; for the calorimetric analysis a Perkin Elmer DSC7 instrument was used, with a rate of 20 °C/min from 30 to 300 °C. The powder X-ray diffraction spectra were obtained with a Philips PW 1050/25 instrument.

Magnetic susceptibilities were measured at room temperature using a Bruker B MB4 electrobalance with $Hg[Co(SCN)_4]$ as calibrant and with correction for diamagnetism with the appropriate Pascal's constants.

X-band ESR measurements on solid samples were carried out with a Bruker 220D-SRC spectrometer, with diphenylpicrylhydrazyl (dpph) as a field marker.

For TEM analysis the powders were ground in a mortar and suspended in ethanol; a drop of suspension was applied to a carbon film supported on a copper grid. Specimens were examined with a Philips EM 400T electron microscope, equipped with an EDAX detector.

Synthesis of organotin hexacyanoferrates

All preparations involved the same general procedure. An aqueous solution containing an excess of potassium hexacyanoferrate (II, III) with respect to the desired reaction stoichiometry was added to a stirred solution of organotin chloride in ethanol. A gelatinous precipitate was formed immediately in all cases, and was filtered off after 10 min. The isolated solid was washed sequentially with water, acetone, and diethyl ether. The products are practically insoluble in all common solvents, except for $(SnPh_3)_3Fe(CN)_6 \cdot 2H_2O$ and $(SnPh_3)_4Fe(CN)_6$ which are soluble in DMSO.

Results and discussion

Physical and analytical data for the six new organotin hexacyanoferrates are given in Table 1. Except for the synthesis of $K_3[SnPh_2(OH)]Fe(CN)_6$ (**5**), all reactions resulted in the complete elimination of KCl. The extremely low solubility of the complexes in all common solvents prevented investigation of the chemical and structural nature of the complexes in solution and also the production of crystals suitable for X-ray diffraction. Our studies were therefore confined to a structural analysis of the solid compounds by spectroscopic and other physical methods.

Table 1

Physicochemical and analytical data [a]

	C (%)	H (%)	N (%)	Sn (%)	Fe (%)	Colour	
						r.t.	140 °C
(1) $(SnPh_3)_3Fe(CN)_6 \cdot 2H_2O$	55.5	3.5	6.6	25.9	5.0	brown	brown
	(55.5)	(3.8)	(6.5)	(27.5)	(4.3)		
(2) $(SnPr_3)_3Fe(CN)_6 \cdot H_2O$	40.5	6.6	8.7	38.7	8.8	brown	grey
	(40.7)	(6.7)	(8.6)	(36.7)	(5.7)		
(3) $(SnBu_2)_3[Fe(CN)_6]_2 \cdot 4H_2O$	35.6	4.8	14.0	27.7	8.2	brown	pale-blue
	(36.2)	(5.2)	(14.1)	(29.9)	(9.4)		
(4) $(SnBu_2)_2Fe(CN)_6 \cdot 2H_2O$	36.9	5.2	11.7	32.5	7.5	white	pale-blue/grey
	(37.0)	(5.6)	(11.8)	(33.3)	(7.8)		
(5) $K_3[SnPh_2(OH)]Fe(CN)_6$	34.4	2.1	13.7	20.0	8.6	brown	pale-blue
	(34.9)	(1.8)	(13.6)	(19.2)	(8.8)		
(6) $(SnPh_3)_4Fe(CN)_6$	58.4	3.7	5.1	29.1	4.4	white	cream
	(58.5)	(3.8)	(4.5)	(29.5)	(3.5)		

[a] Calculated values are given in parentheses.

After some months, or after thermal treatment at ca. 140 °C for 2 hours, some compounds exhibit a noticeable change in colour (Table 1). The ν(CN) stretch observed in the solid state for room temperature and thermally treated samples (110–140 °C) are given in Table 2. Stretching frequencies higher than those for $K_3Fe(CN)_6$ or $K_4Fe(CN)_6$ have been assigned to linear bridging between metal centres, while lower frequency bands are associated with terminal or non-linearly bridging CN groups [10–12]. In this respect it is noteworthy that thermal treatment of the Fe^{II} complexes has little or no effect, while similar treatment of the Fe^{III} compounds causes an appreciable increase in the intensity of ν(CN) at lower frequency at the expense of higher frequency bands (Fig. 1); this increase possibly arises from partial and gradual reduction of the oxidation state of the iron.

The main peaks observed in the X-ray powder diffraction patterns are listed in Table 3. All the compounds were studied both as the products of room temperature

Table 2

The ν(CN) frequency values (cm^{-1}) at room temperature and in the 110–140 °C range [a]

	r.t.	110 °C (1 h 15′)	120 °C (2 h 10′)	140 °C (2 h 10′)
(1) $(SnPh_3)_3Fe(CN)_6 \cdot 2H_2O$	2140 s	2140 s(−)	2140 ms(−)	2140 ms(−)
	2080 w(br)	2070 m(br)(+)	2070 s(br)(+)	2070 s(br)(+)
(2) $(SnPr_3)_3Fe(CN)_6 \cdot H_2O$	2140 s	2170 vw	2170 vw [b]	2170 vw [b]
	2080 s(br)	2085 s(br)	2085 s(br)	2085 s(br)
(3) $(SnBu_2)_3[Fe(CN)_6]_2 \cdot 4H_2O$	2140 s	2140 s(−)	2175 vw	2175 vw [b]
	2080 s	2080 s(+)	2080 vs(+)	2080 vs
(4) $(SnBu_2)_2Fe(CN)_6 \cdot 2H_2O$	2075 s(br)	2075 s(br) [b]	2075 s(br) [b]	2075 s (br) [b]
(5) $K_3[SnPh_2(OH)]Fe(CN)_6$	2075 s(br)	2075 s(br) [b]	2075 s(br) [b]	2075 s(br) [b]
(6) $(SnPh_3)_4Fe(CN)_6$	2090 s	2090 s [b]	2090 s [b]	2090 s [b]
	2040 s	2040 s	2040 s	2040 s

[a] $K_3Fe(CN)_6$: 2120 cm^{-1}; $K_4Fe(CN)_6$: 2090 cm^{-1}. (−) and (+) mean a decrease and an increase of the intensity of the band respectively. [b] Unchanged with respect to the preceding value.

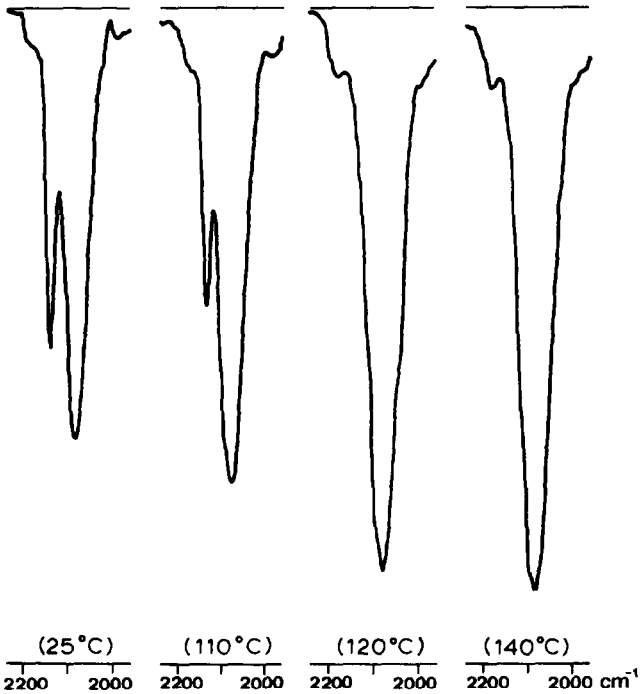

Fig. 1. The effect of the thermal treatment on the ν(CN) bands in $(SnBu_2)_3[Fe(CN)_6]_2 \cdot 4H_2O$.

Table 3
Main peaks in the X-ray diffraction powder patterns

	r.t.	110 °C (1 h 15′)	120 °C (2 h 10′)	140 °C (2 h 10′)
(1) $(SnPh_3)_3Fe(CN)_6 \cdot 2H_2O$	7.952	7.955	8.067	8.320
	13.778	13.797	13.977	14.450
	15.941	15.974	16.199	16.743
	17.846	17.899	18.146	18.679
(2) $(SnPr_3)_3Fe(CN)_6 \cdot H_2O$	8.535	8.550	8.571	8.716
	14.759	14.783	14.916	15.012
	17.054	17.077	17.183	17.451
	19.057	19.139	19.226	19.495
(3) $(SnBu_2)_3[Fe(CN)_6]_2 \cdot 4H_2O$	7.486	7.516	7.531	7.584
	14.542	14.589	14.644	14.794
	18.518	18.611	18.743	18.807
	19.970	20.044	20.268	20.384
(4) $(SnBu_2)_2Fe(CN)_6 \cdot 2H_2O$	10.586	24.762 [a]	24.762	24.721 [b]
	21.179	29.986	29.997	29.955
	30.684	31.489	31.500	31.472
	31.968			
(5) $K_3[SnPh_2(OH)]Fe(CN)_6$	30.582	24.754 [a]		
	31.925	29.981	amorphous	amorphous
		31.464		
(6) $(SnPh_3)_4Fe(CN)_6$	5.777	5.848	5.790 [b]	5.797
	13.544	13.564	13.552	13.557
	17.549	17.568	17.560	17.563
	21.357	21.380	21.360	21.366

[a] Change of the crystalline structure. [b] Decrease of θ with the temperature.

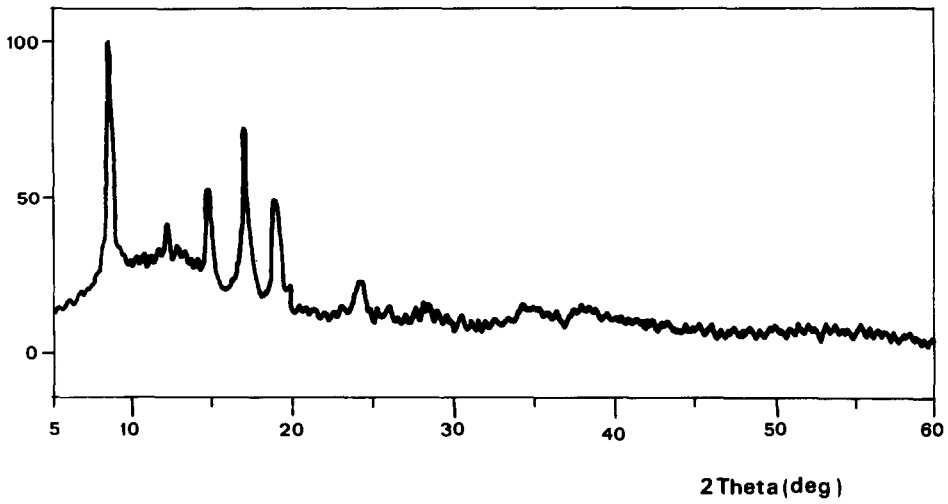

Fig. 2. The X-ray powder diffraction pattern of $(SnPr_3)_3Fe(CN)_6 \cdot H_2O$.

syntheses and after thermal treatment (110–140 °C), and in all cases a crystalline phase superimposed upon an amorphous phase was observed, keeping with the probable polymeric nature of the materials. Thermal treatment causes a decrease (and in some cases complete disappearance) of the crystalline phase, and concomitant peak shift to higher θ values for the remaining crystalline phase, corresponding to a collapse in crystal structure following solvent loss (vide infra).

Interestingly, the anhydrous compound **6** does not behave in this way (Table 3), while both **5** and **4** show evidence for the formation of a second crystalline phase after thermal treatment (Table 3, Fig. 2). In general, though, the higher the temperature or the longer the duration of thermal treatment, the more significant the changes in the diffraction patterns.

Thermogravimetric analysis (TG) in the 30–400 °C range reveals similar behaviour for all the compounds (Fig. 3). Complete loss of water occurs from the five hydrated compounds below 100 °C. Between 100 and ca. 250 °C the weight of the sample remains practically constant, then at ca. 250 °C total decomposition of the organic moiety accompanied by gradual, but incomplete, loss of cyano groups occurs, as evidenced by the infrared spectra of thermally treated samples. Beyond ca. 330 °C, all thermograms show a residual gradient attributable to slow and continuous decomposition of the cyano groups.

In the case of $(SnBu_2)_3[Fe(CN)_6]_2 \cdot 4H_2O$, the residue from the thermogravimetric analysis under nitrogen, interrupted at 400 °C, was investigated by elemental microanalysis and transmission electron microscopy (TEM). This material is an amorphous, homogeneous black powder, with particles of various sizes (most of them ranging with diameters between 5 and 50 nm), as shown in the TEM view of Fig. 4. The Sn/Fe ratio, deduced by energy dispersive X-ray microanalysis, carried out on different zones of the sample, is invariably 1.5, as in the starting material; on the basis of C, N elemental microanalysis, its tentative formulation is $Sn_3Fe_2(CN)_7$.

Thermal decomposition in air at 800 °C produces a brick-red microcrystalline powder. TEM investigations have revealed that segregation of tin oxide (SnO_2, from X-ray powder pattern) from iron oxide occurs.

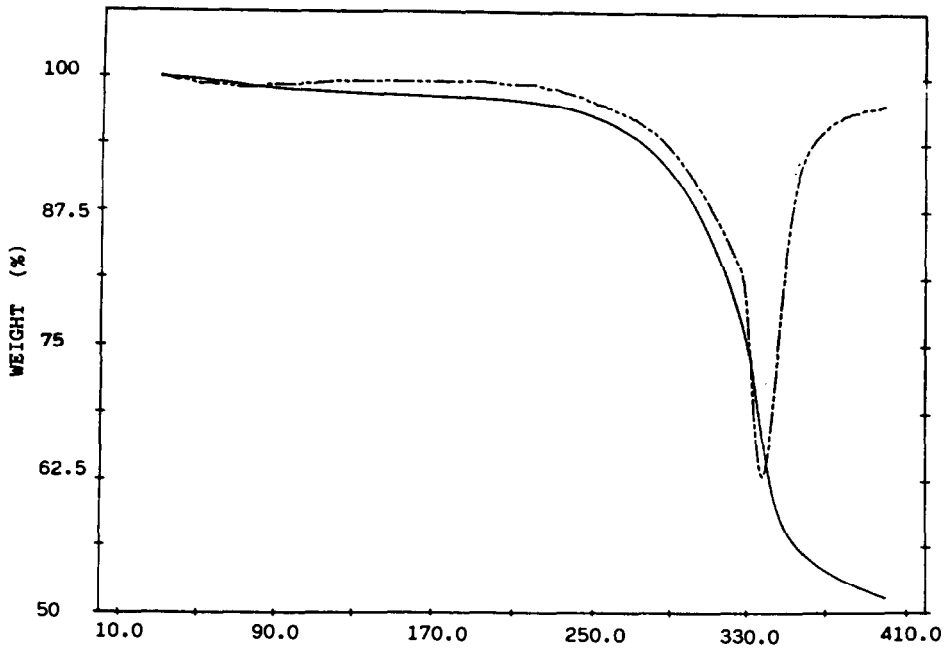

Fig. 3. The thermogravimetric pattern of $(SnBu_2)_3[Fe(CN)_6]_2 \cdot 4H_2O$.

In contrast to constancy of the TG behaviour, substantial differences appear in the corresponding differential scanning calorimetric (DSC) experiments. In particular, three different patterns of behaviour were observed, namely (i) strong heat absorption: $K_3[SnPh_2(OH)]Fe(CN)_6$, 114.1 Jg^{-1}; $(SnBu_2)_2Fe(CN)_6 \cdot 2H_2O$, 125.8 Jg^{-1} (Fig. 5), (ii) heat loss: $(SnPh_3)_3Fe(CN)_6 \cdot 2H_2O$, -76.8 Jg^{-1}; $(SnPr_3)_3Fe(CN)_6 \cdot H_2O$, -46.4 Jg^{-1}; $(SnBu_2)_3[Fe(CN)_6]_2 \cdot 4H_2O$, -22.5 Jg^{-1} (Fig. 5), (iii) no heat change: $(SnPh_3)_4Fe(CN)_6$.

Two features emerge from these data. The first is that compounds that show heat absorption in the DSC experiments also show a change in crystalline phase upon heat treatment through their powder diffraction patterns, phenomena which can be rationalised in terms of a phase change associated with a melting process. The second is that heat loss in the DSC occurs for all the Fe^{III} compounds, which also show peak shifts to higher θ after heat treatment in their diffraction patterns, and also the greatest change in $\nu(CN)$ upon heat treatment. Such changes can be plausibly attributed to a thermal rearrangement to a more stable solid lattice. Finally, $(SnPh_3)_4Fe(CN)_6$ is the most structurally stable of the compounds synthesised, showing no thermic exchange in the DSC, and giving infrared spectra and X-ray powder patterns which do not change upon heat treatment of the sample.

All of the Fe^{II} complexes studied are diamagnetic. This is typical of low-spin Fe^{II} in a strong ligand field such as $[Fe(CN)_6]^{4-}$. The magnetic moments observed in **1**, **2**, and **3** (μ_{eff} in 2.2–2.3 B.M. range) are characteristic of low-spin Fe^{III} compounds [13]. The very broad lines in the room-temperature ESR spectra prevent assessment of them. At 110 K a rhombic type of ESR spectra (Fig. 6) with three g-values, very similar for all the compounds ($g = 2.3, 2.1, 1.9$; $g = 2.3, 2.18, 1.91$; $g = 2.29, 2.05, 1.88$ for **1**, **2** and **3** respectively) is observed, and corresponds to low-spin Fe^{III} compounds [14].

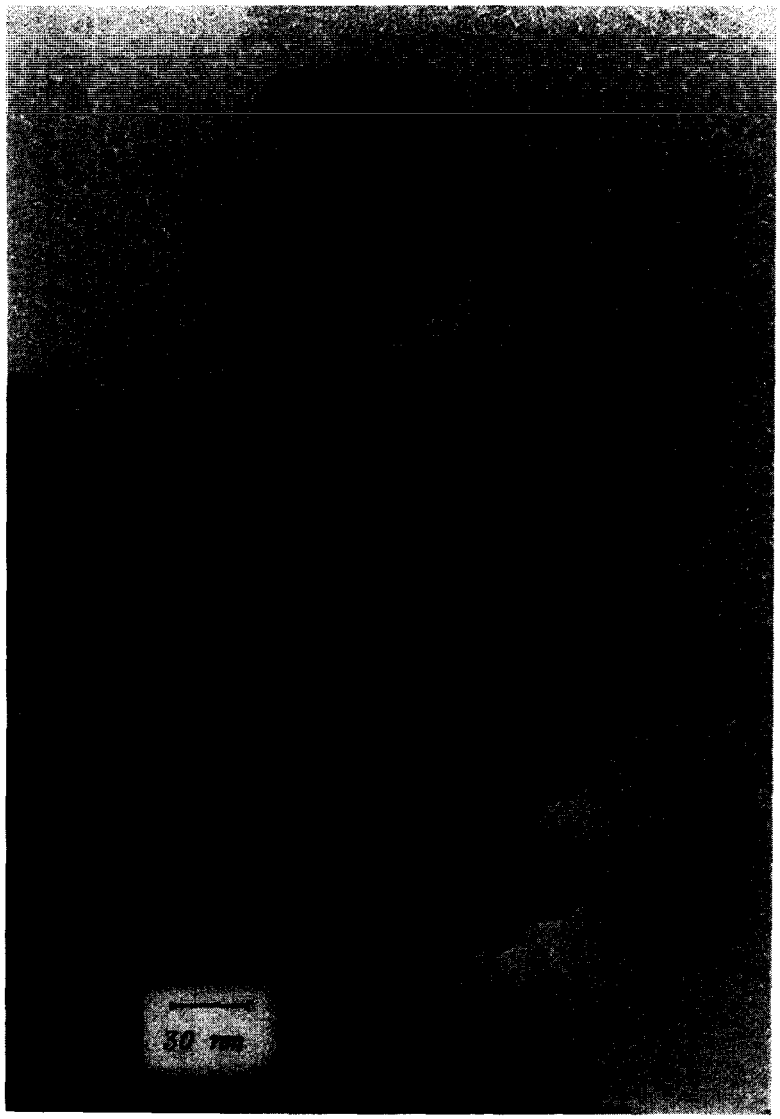

Fig. 4. Transmission electron microscope (TEM) view of the amorphous powder obtained by decomposition of $(SnBu_2)_3$ $[Fe(CN)_6]_2 \cdot 4H_2O$ under nitrogen at 400 °C.

A weak signal at $g = 4.3$ is also observed. This last peak is known to be characteristic of rhombically distorted high-spin iron(III) [15,16], and it has been reported that it can be obtained even from negligible amounts of Fe^{III} [17].

Evidence for the electronic and structural nature of the complexes comes from ^{57}Fe and ^{119}Sn Mössbauer spectroscopies (Table 4), but the results are by no means unambiguous. All of the Fe^{II} compounds **4–6** appear as singlets in the ^{57}Fe Mössbauer spectra, or in the case of **6** as a very narrow doublet. This is typical of low spin Fe^{II} systems of this type, while the lowering of O_h symmetry in the case of **6** is similar to that induced in the spectrum of $H_4Fe(CN)_6$ (0.28 mm s^{-1} [18]) by a

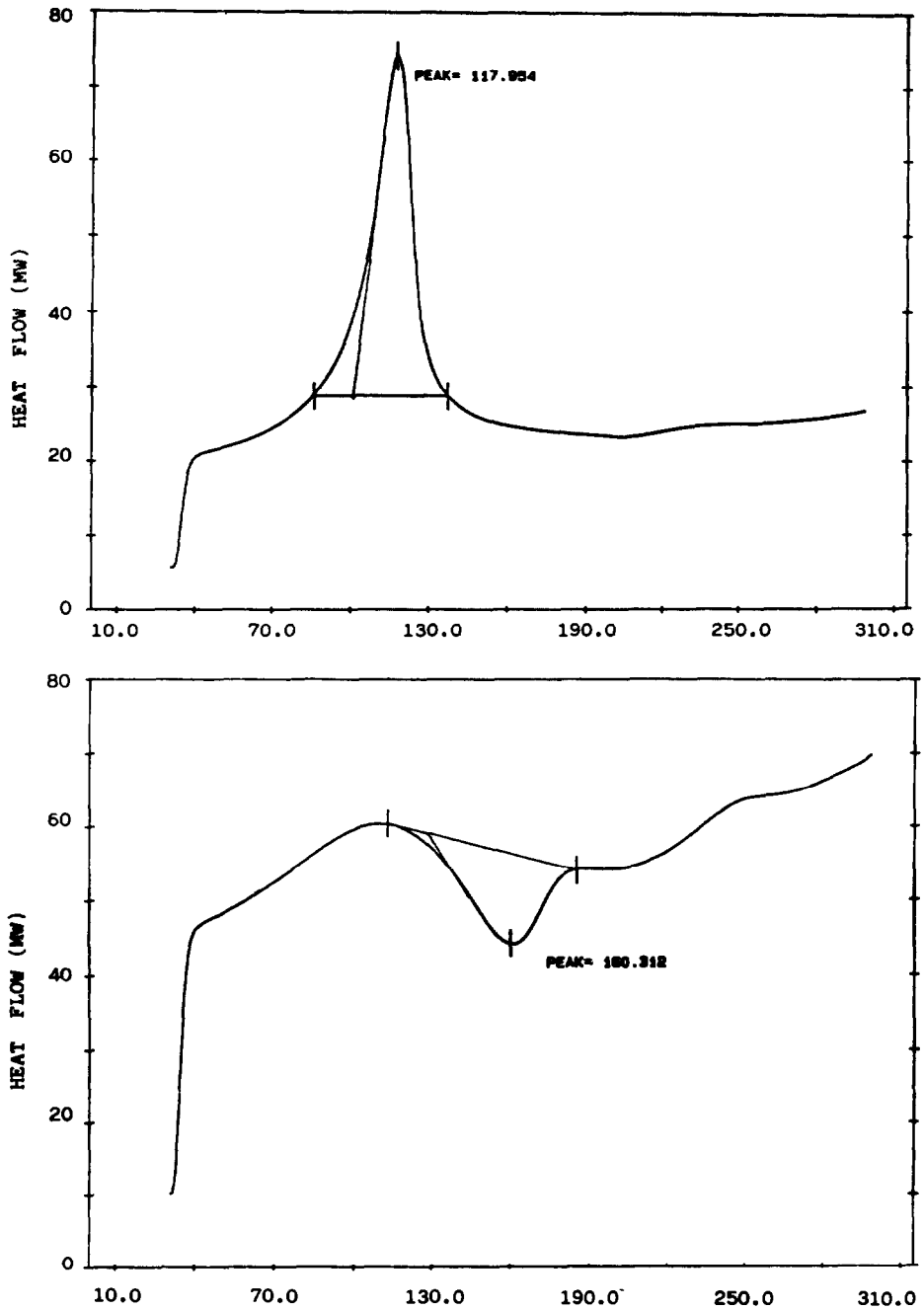

Fig. 5. The differential scanning calorimeter pattern of $(SnBu_2)_2Fe(CN)_6 \cdot 2H_2O$ and $(SnBu_2)_3[Fe(CN)_6]_2 \cdot 4H_2O$.

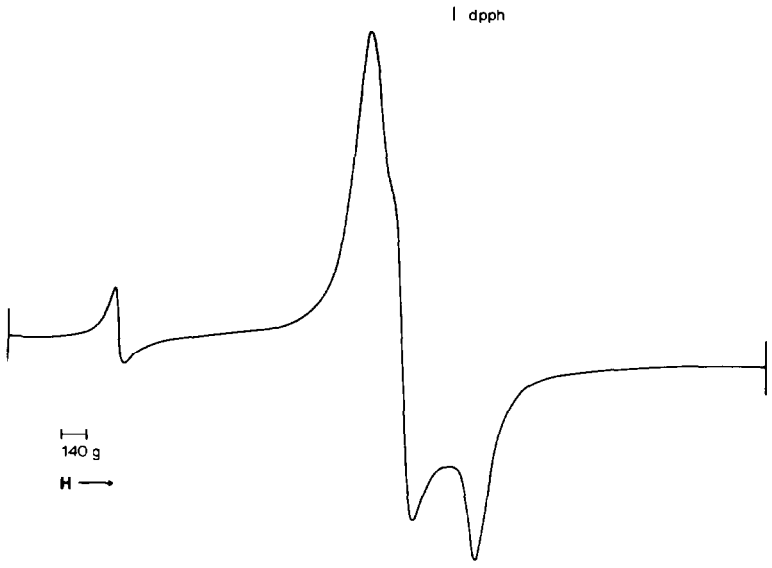

Fig. 6. ESR spectrum at 110 K of $(SnPr_3)_3Fe(CN)_6 \cdot H_2O$.

hydrogen bonded lattice. These results thus support the diamagnetic nature of the complexes, and are typical of iron in a strong ligand field.

The spectra of the Fe^{III} compounds are more complex, and the interpretation of the data less certain. All the spectra show both a quadrupole split doublet with a singlet of similar isomer shift superimposed (Fig. 7). The doublet is typical of low spin Fe^{III} and other known ferricyanide complexes give q.s. values in the range 0.2–1.6 mm s^{-1} [19]. Again, these results are consistent with the measured magnetic moments of 2.2–2.3 B.M. and the typically rhombic-type ESR spectra. The singlet in the ^{57}Fe Mössbauer spectra of the Fe^{III} is of less certain origin. In the ESR spectra only a weak signal is present, at $g = 4.3$, which is characteristic of rhombi-

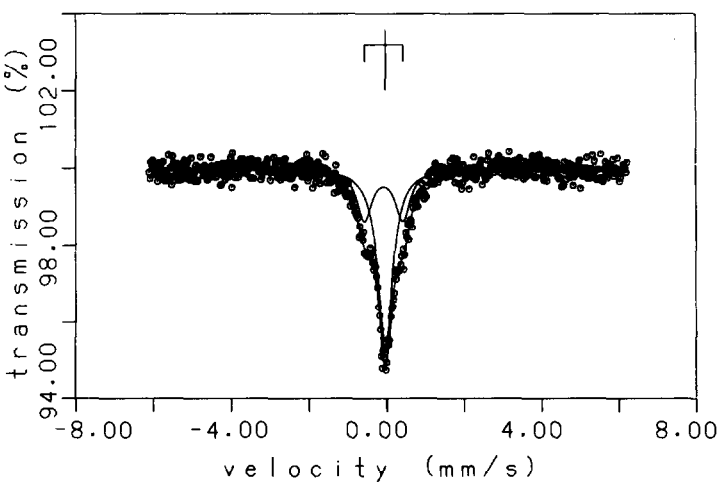

Fig. 7. ^{57}Fe Mössbauer spectrum of $(SnBu_2)_3[Fe(CN)_6]_2 \cdot 4H_2O$.

Table 4

^{57}Fe and ^{119}Sn Mössbauer spectroscopic data

Compound	i.s.	q.s.	Γ	%
^{57}Fe Mössbauer data				
(1) $(SnPh_3)_3Fe(CN)_6 \cdot 2H_2O$ [a]	−0.09	1.28	0.55 [b]	86
	−0.01		0.59	14
(2) $(SnPr_3)_3Fe(CN)_6 \cdot H_2O$ [a,c]	−0.06	0.82	0.45 [b]	22
	−0.02		0.48	78
(3) $(SnBu_2)_3[Fe(CN)_6]_2 \cdot 4H_2O$ [a]	−0.07	0.99	0.47 [b]	36
	−0.03		0.45	64
(4) $(SnBu_2)_2Fe(CN)_6 \cdot 2H_2O$	−0.04		0.40	100
(5) $K_3[SnPh_2(OH)]Fe(CN)_6$	−0.05		0.39	100
(6) $(SnPh_3)_4Fe(CN)_6$	−0.02	0.25	0.35 [b]	100
^{119}Sn Mössbauer data				
(1) $(SnPh_3)_3Fe(CN)_6 \cdot 2H_2O$	1.26	3.50	0.90, 0.94	100
(2) $(SnPr_3)_3Fe(CN)_6 \cdot H_2O$	1.37	3.55	0.87, 1.10	100
(3) $(SnBu_2)_3[Fe(CN)_6]_2 \cdot 4H_2O$ [d]	1.56	4.45	0.88 [b]	51
	1.36	3.30	1.07 [b]	31
	0.49	2.08	0.95 [b]	18
(4) $(SnBu_2)_2Fe(CN)_6 \cdot 2H_2O$	1.18	3.18	0.99, 1.12	100
(5) $K_3[SnPh_2(OH)]Fe(CN)_6$	1.03	2.86	1.18, 1.29	100
(6) $(SnPh_3)_4Fe(CN)_6$	1.19	2.95	1.16, 1.09	100
"2 site fit [e]	1.24	3.08	1.04 [b]	81
	1.17	2.40	1.06 [b]	29

[a] Two site fit. [b] FWHH for the two wings of the doublet constrained to be equal. [c] A singlet fit is statistically much poorer, and the line is very broad. [d] Three site fit. [e] Gives a slightly better goodness-of-fit than the single site, but the difference is very small and may not be significant.

cally distorted high-spin Fe^{III}. However, the singlet is the dominant feature of the Mössbauer spectra of **2** and **3** and a significant contributor to the spectrum of **1**, not a minor impurity in the spectra of the three compounds as suggested by ESR, so other explanation must be found. The appearance of the spectra as a whole are remarkably similar to those for $K_3Fe(CN)_6$ under high pressure [20], which also show a ferrocyanide-type singlet in addition to a Fe^{III} doublet. It is, however, difficult to rationalise the products in terms of a chemical redox reaction during synthesis, or with known physical methods of reduction such as photochemically at 1 atmosphere [21] or a combination of high pressure and shear [22]. However, it would seem from the limited data available that the origin of the Mössbauer singlet in these formally Fe^{III} species is related to the intensity of the IR band at ca. 2080 cm^{-1}, nominally associated with $Fe(CN)_6^{4-}$.

All the ^{119}Sn Mössbauer spectra (Table 4) confirm that tin is in the +4 oxidation state, and they provide additional information regarding the coordination polyhedron surrounding tin in the complexes. The spectra of compounds **1**, **2** and **6** all consist of a simple doublet. For **1** and **2**, the value of the q.s. (3.50, 3.55 mm s^{-1}) is typical of a trigonal bipyramidal geometry at tin with equatorial hydrocarbon groups. Direct comparison can be made with data for $(SnMe_3)_3Co(CN)_6$ (q.s. = 3.84 mm s^{-1} [23]), for which X-ray crystallographic data confirm the proposed geometry about tin. It appears that for the triorganotin complexes the coordination about tin is independent of the different types of iron site (Table 4) in the lattice.

For **6**, the diminished q.s. data appear to suggest a similar situation, but with a geometry about tin between that of tetrahedral and trigonal bipyramidal.

For the diorganotin compounds **4** and **5**, the q.s. data cannot unambiguously distinguish *cis*-R_2SnX_3 from distorted *trans*-R_2SnX_4 arrangements, though an estimate of the C–Sn–C angle of ca. 130° can be made in each of the two cases [24].

The spectrum of **3** is complex, and seems to fit well to three tin sites (doublets), though no doubt other possibilities could be found based simply on goodness-of-fit criteria. One site (q.s. = 4.45 mm s^{-1}) would correspond to a perfect *trans*-$R_2Sn(CN)_4$ coordination sphere, with a linear (or nearly so) C–Sn–C fragment. The second site (q.s. = 3.30 mm s^{-1}) is similar to **4** and **5** above, and the data can be interpreted similarly. Interestingly, the ratio of the two types of tin site (assuming equal recoil-free fractions) is ca. 60 : 40, which is also the ratio of Fe^{III}: pseudo-Fe^{II} (doublet : singlet) in the ^{57}Fe spectra. It is tempting therefore to associate a specific diorganotin site with a particular iron site in the lattice, in contrast to the case for the triorganotin compounds **1**, **2** discussed above. The final, low intensity component has a q.s. very similar to that of $SnBu_2O$, though the i.s. is markedly different from that in the literature (1.04 mm s^{-1}).

From the correlation of the chemical and structural data and mainly from the results of the ^{119}Sn and ^{57}Fe Mössbauer studies some suggestions about their structure can be advanced. Firstly, in agreement with the low solubility in all common solvents we attribute a polymeric nature to all the compounds, and this is favoured by the bridging behaviour of some cyano groups; it is impossible to establish the presence of one-, two- or three-dimensionally linked coordinative polymers.

The comparison of all the spectroscopic and physicochemical results reveals some chemical and physical similarities which can be associated with structural analogies. The strong similarities in the effects produced by the thermal treatment are well evident in $(SnPh_3)_3Fe(CN)_6 \cdot 2H_2O$ and $(SnPr_3)_3Fe(CN)_6 \cdot H_2O$ in agreement with the presence of a tbp geometry.

The other iron(III) complex shows some differences from the above mentioned complexes, and this may arise from the probable six-coordinate tin environment. A common structural feature is also present in two of the iron(II) complexes, $(SnBu_2)_2Fe(CN)_6 \cdot 2H_2O$ and $K_3[SnPh_2(OH)]Fe(CN)_6$, in which a *cis*-R_2SnX_3 environment seems to be present.

Acknowledgement

We thank Dr. Simona Bigi (University of Modena) for skilled assistance in performing the TEM analyses.

References

1 C. Pelizzi, G. Pelizzi and P. Tarasconi, J. Organomet. Chem., 28 (1985) 403.
2 D. Franzoni, G. Pelizzi, G. Predieri, P. Tarasconi, F. Vitali, C. Pelizzi, J. Chem. Soc., Dalton Trans., (1989) 247.
3 C. Carini, C. Pelizzi, G. Pelizzi, G. Predieri, P. Tarasconi, F. Vitali, J. Chem. Soc., Chem. Commun., (1990) 613.
4 G. Boxhoorn, J. Moolhuysen, J.G.F. Goolegem, R.A. van Santen, J. Chem. Soc., Chem. Commun., (1985) 1305.

5 R. Usón, J. Fornies, M.A. Usón, E. Lalinde, J. Organomet. Chem., 185 (1980) 359.
6 K. Yünlü, N. Höck, R.D. Fischer, Angew. Chem., Int. Ed. Engl., 24 (1985) 879.
7 P. Brandt, A.K. Brimah, R.D. Fischer, Angew. Chem., Int. Ed. Engl., 27 (1988) 1521.
8 M. Adam, A.K. Brimah, R.D. Fischer, and L. Xing-Fu, Inorg. Chem., 29 (1990) 1597.
9 K.C. Molloy, T.G. Purcell, K. Quill, I.W. Nowell, J. Organomet. Chem., 267 (1984) 237.
10 M. Wicholas, T. Wolford, Inorg. Chem., 13 (1974) 316.
11 O.P. Anderson, Inorg. Chem., 14 (1975) 730.
12 J. Metz, M. Hanack, J. Am. Chem. Soc., 105 (1983) 828.
13 E.A. Boudreaux, L.N. Mulay, Theory and Application of Molecular Paramagnetism, Wiley and Sons, New York, 1976.
14 A. Abragam, B. Bleaney, Electron Paramagnetic Resonance of Transition Ions, Oxford University Press, England, 1970.
15 J. Peisach, W.E. Blumberg, E.T. Lode, M.J. Coon, J. Biol. Chem., 246 (1971) 5877.
16 S.A. Cotton, J.F. Gibson, J. Chem. Soc. A, (1971) 803.
17 R. Aasa, S.P.J. Albracht, K.E. Falk, B. Lanne, T. Vanngaed, Biochim. Biophys. Acta, 422 (1976) 260.
18 A.N. Garg and P.S. Goel, J. Inorg. Nucl. Chem., 31 (1969) 697.
19 N.N. Greenwood and T.C. Gibb, Mössbauer Spectroscopy, Chapman and Hall, London, 1971.
20 A.R. Champion and H.G. Drickamer, J. Chem. Phys., 47 (1967) 2591.
21 W.P. Griffith, Quart. Rev. (London), 16 (1962) 188.
22 H.A. Larsen and H.G. Drickamer, J. Phys. Chem., 61 (1957) 1249.
23 K. Yunlii, N. Hock, and R.D. Fischer, Angew. Chem., Int. Ed. Engl., 24 (1985) 879.
24 T.K. Sham and G.M. Bancroft, Inorg. Chem., 14 (1975) 2281.